Cross Calibration of the Landsat-7 ETM+ and EO-1 ALI Sensor

Gyanesh Chander, David J. Meyer, and Dennis L. Helder, *Member, IEEE*

***Abstract*—As part of the Earth Observer 1 (EO-1) Mission, the Advanced Land Imager (ALI) demonstrates a potential technological direction for Landsat Data Continuity Missions. To evaluate ALI's capabilities in this role, a cross-calibration methodology has been developed using image pairs from the Landsat-7 (L7) Enhanced Thematic Mapper Plus (ETM+) and EO-1 (ALI) to verify the radiometric calibration of ALI with respect to the well-calibrated L7 ETM+ sensor. Results have been obtained using two different approaches. The first approach involves calibration of nearly simultaneous surface observations based on image statistics from areas observed simultaneously by the two sensors. The second approach uses vicarious calibration techniques to compare the predicted top-of-atmosphere radiance derived from ground reference data collected during the overpass to the measured radiance obtained from the sensor. The results indicate that the relative sensor chip assemblies gains agree with the ETM+ visible and near-infrared bands to within 2% and the shortwave infrared bands to within 4%.**

***Index Terms*—Bands, Brookings, characterization, Earth Observing 1 (EO-1) Advanced Land Imager (ALI), Landsat Data Continuity Missions, Landsat radiance, Landsat-7 (L7) Enhanced Thematic Mapper Plus (ETM+), radiometry, Railroad Valley Playa, relative spectral response (RSR), sensor chip assembly (SCA), shortwave infrared (SWIR), spectral, vicarious calibration, visible near-infrared (VNIR), White Sands.**

I. Introduction

THE ABILITY to detect and quantify changes in the earth's environment depends on satellites that can provide calibrated, consistent measurements of earth's surface features. Such changes over time are monitored using multiple generations of imaging sensors whose operational lifetimes are phased over years and decades. A critical step in this process is the calculation of radiance in order to put image data from subsequent generations of sensors onto a common radiometric scale. Consistency of radiance measurements between two different sensors starts with sound calibration of the individual sensors. For those missions whose operational lifetimes overlap, post-launch cross calibration can make use of nearly simultaneous imaging of pseudoinvariant features on the surface of the earth or moon as common targets.

Manuscript received November 30, 2003; revised April 10, 2004. This work was supported in part by the National Aeronautics and Space Administration and in part by the U.S. Geological Survey of the Department of the Interior under Grant NRA-99-OES-01.

G. Chander and D. J. Meyer are with the Science Application International Corporation, Earth Resources Observation System Data Center, U.S Geological Survey, Sioux Falls, SD 57198 USA (e-mail: gchander@usgs.gov).

D. L. Helder is with the Electrical Engineering and Computer Science Department, South Dakota State University, Brookings, SD 57007 USA (e-mail: Dennis.Helder@sdstate.edu).

Digital Object Identifier 10.1109/TGRS.2004.836387

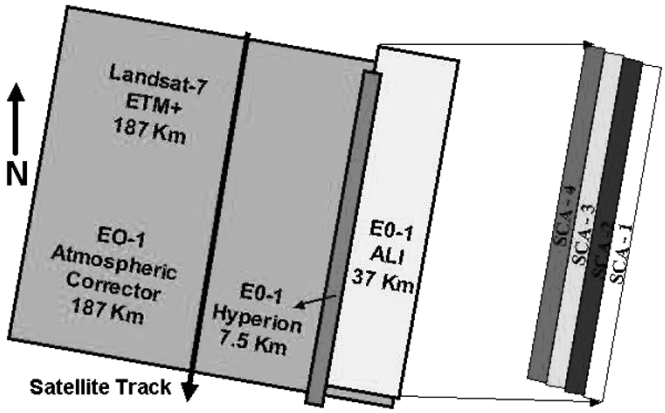

Fig. 1. EO-1 and L7 swath covered on the ground.

A. Instrument Overview

The Enhanced Thematic Mapper Plus (ETM+) was launched on April 15, 1999 on the L7 platform; it is based on the Thematic Mapper (TM) sensor onboard the Landsat-4 and Landsat-5 instruments. These instruments achieve a 185-km cross-track ground swath by using a bidirectional scan mirror to traverse the instrument line-of-sight through a 15° cross-track field of view (FOV). The Advanced Land Imager (ALI) was launched on November 21, 2000 on the Earth Observing 1 (EO-1) platform. It uses wide-angle optics designed to provide a continuous FOV without the use of a scan mirror. Although ALI's focal plane is designed to support a 15° FOV, only a 3° FOV was populated with linear detector arrays arranged in four sensor chip assemblies (SCAs). The partially populated ALI provides a ground swath width of 37 km, as shown in Fig. 1. Each SCA contains 320-element detector arrays that image in nine multispectral bands with 30-m spatial resolution, as well as a 960-element detector array that images a single panchromatic band [1].

EO-1 passes over a given target approximately 1 min after L7 in a sun-synchronous, 705-km orbit with a 10:01 A.M. descending node. In this configuration, both instruments view identical targets on the earth's ground surface in order to verify the spatial, spectral, and radiometric performance of ALI with respect to the well-calibrated ETM+. As a technological demonstration mission, ALI improves upon the ETM+ design in several ways. Table I compares various features of the EO-1

TABLE I
PHYSICAL SPECIFICATION OF EO-1 ALI AND L7 ETM+ INSTRUMENTS [1]

EO-1/L7 Instrument Comparison		
Physical Unit	**L7 (ETM+)**	**EO-1 (ALI)**
Mass (kg)	425	100
Power (W)	545	100
Size (m^3)	1.4	0.2
Bands	7	10
Detectors per band	16	1280
Thermal band	1	None
Data rate (Mbps)	150	300
Pan Resolution (m)	15	10
Relative SNR	1x	4x

ALI to the L7 ETM+ instrument. In terms of instrument size, ALI is one-fourth of the mass and approximately one-third of the volume of ETM+. Functionally, it uses approximately one-fifth of the power required by ETM+. Radiometrically, ALI is designed to operate without saturation over the full range of albedo with 12-bit resolution. In addition, the SNR is between four and ten times larger than SNR for ETM+ in the bands common to both sensors [1].

The in-flight radiometric calibration for both of the sensors includes regular data collection from the onboard internal calibration source, periodic solar observation, and repeated viewing of standard earth scenes. ALI also includes periodic lunar observations. To maintain consistency, L7 and EO-1 are referred to as instruments, and ETM+ and ALI are respectively referred to as sensors throughout this paper.

B. Relative Spectral Response Profiles

The relative spectral response (RSR) profiles between corresponding ETM+ and ALI spectral bands are shown in Fig. 2. The wavelength coverage and ground sample distance (GSD) are summarized in Table II. The ALI bands were designed to mimic the six standard ETM+ spectral bands 1, 2, 3, 4, 5, and 7; three new bands were added in order to more effectively address atmospheric interference effects in specific applications. The ALI prime bands are the 1p, 4p, and 5p. The prime means the "nonlegacy" bands, and is represented with the extension "p." One of the new bands (1p) is a deep blue to near-ultraviolet band used in atmospheric correction and oceanography studies. Bands 4 and 4p are positioned to avoid the water absorption feature affecting ETM+ band 4. Band 5p is an additional SWIR band used in vegetation mapping applications. Finally, the ALI panchromatic band attenuates beyond red in order to allow more accurate identification of vegetation than is possible with the ETM+ panchromatic band, which extends into the near infrared. The ALI bands that were designed to mimic the standard ETM+ spectral bands 1, 2, 3, 5, and 7 were used in this study. ETM+ band 4 was not taken into consideration because the respective spectral response in ALI was divided into two narrower bands, 4 and 4p.

C. Test Site Descriptions

The test sites used for sensor calibration of the solar reflective bands are primarily located in desert regions. These regions

TABLE II
SPECTRAL COVERAGE AND GSD OF (a) THE L7 ETM+ AND (b) THE EO-1 (ALI) SENSOR

(a) Landsat 7 ETM+

Band	Spectral Range (μm)	GSD (m)
Pan	0.520 - 0.900	15
1	0.450 - 0.515	30
2	0.525 - 0.605	30
3	0.630 - 0.690	30
4	0.775 - 0.900	30
5	1.550 - 1.750	30
6	10.40 - 12.50	60
7	2.090 - 2.350	30

(b) EO-1 ALI

Band	Spectral Range (μm)	GSD (m)
Pan	0.480-0.690	10
1P	0.433-0.453	30
1	0.450-0.515	30
2	0.525-0.605	30
3	0.630-0.690	30
4	0.775-0.805	30
4P	0.845-0.890	30
5P	1.200-1.300	30
5	1.550-1.750	30
7	2.080-2.350	30

TABLE III
IMAGE PAIRS FROM ALI AND ETM+ SENSORS

Location	Date	DOY	Path/Row
Brookings	Sept. 05, 2001	248	029/029
Railroad Valley	Jun. 30, 2001	181	040/033
White Sands	Mar. 25, 2001	84	033/037

are used for several reasons. First, these sites exhibit high surface reflectance, which decreases uncertainties in the calibration. Second, the low probability of cloud coverage improves the chances of the sensor imaging the test site at the time of overpass. In addition, the low aerosol loading typical of these regions decreases uncertainties due to the atmospheric characterization. The test sites used for the current work are described below [2].

1) *Railroad Valley Playa:* The Railroad Valley Playa is a dry lakebed with a predominantly clay composition. It is a desert site with no vegetation, and aerosol loading is typically low. The test site is located between the cities of Ely and Tonopah, NV at latitude-longitude coordinates 38.5° N and 115.7° W, at an elevation of 1.3 km above sea level. It is referenced in the Worldwide Reference System 2 (WRS-2) with path 40 and row 33.
2) *White Sands Missile Range:* The White Sands Missile Range is relatively devoid of vegetation and has a low aerosol loading. The test site is located in the New Mexico desert at latitude-longitude coordinates 32.9° N and 106.4° W, at an elevation of 1.2 km above sea level. It is referenced in the WRS-2 system with path 33 and row 37.
3) *Brookings:* The Brookings test site is a grass field in Brookings, SD, at latitude-longitudecoordinates 44.3° N and 96.8° W, at an elevation of 0.5 km above sea level. It is referenced in the WRS-2 system with path 29 and row 29.

Table III lists the acquisition date, day-of-year (DOY), path, row, and location of the scenes used for the analysis. The scenes

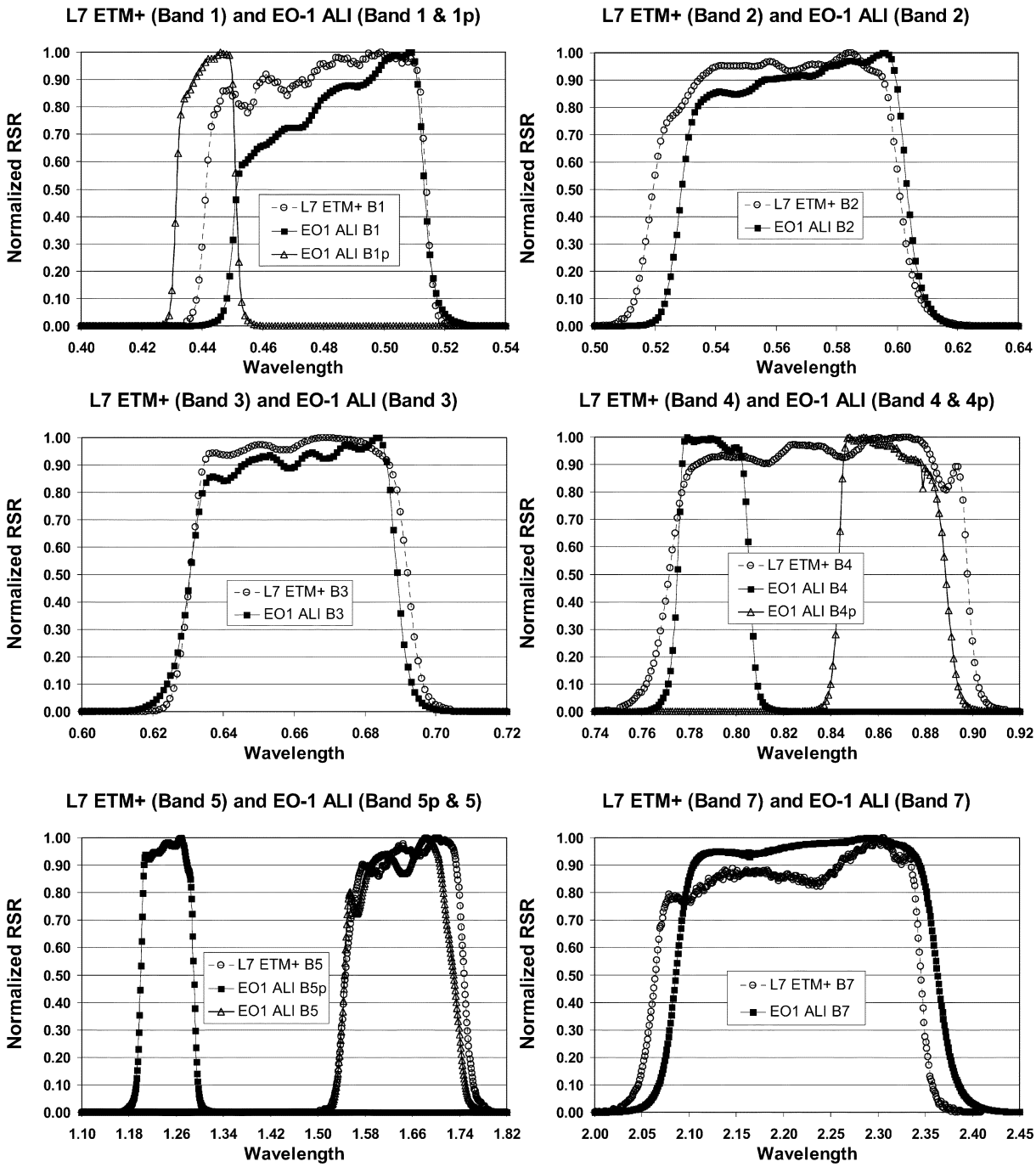

Fig. 2. Relative spectral responses profiles of EO-1 ALI and L7 ETM+.

from Railroad Valley and White Sands were used for calibration by nearly simultaneous surface observations studies. Ground reference data were collected over the Brookings test site, and the scene acquired over Brookings test site were used for the vicarious calibration study.

D. Data Processing System and Conversion to Radiance

Level 1R (L1R) scenes from the ETM+ and ALI sensors were used for this particular study. L1R is a radiometrically corrected product; radiometric artifacts such as detector striping are removed before radiometric correction. During L1R product generation, the image pixels are converted to units of absolute radiance using 32-bit floating-point calculations. The absolute radiance values are then scaled to calibrated digital numbers before output to the distribution media. A scaling factor of 100 for ETM+ and 30 for ALI is used to create these calibrated digital numbers. The ETM+ data were processed through the image assessment system, and the EO-1 ALI data were processed through the EO-1 processing system (version-4.5999 and database December 13, 2001) at the Earth Resources Observation System (EROS) Data Center (EDC).

The sensors do not measure radiances directly but rather record quantities that, once calibrated, are equal to or linearly related to radiances. The detectors exhibit linear response to

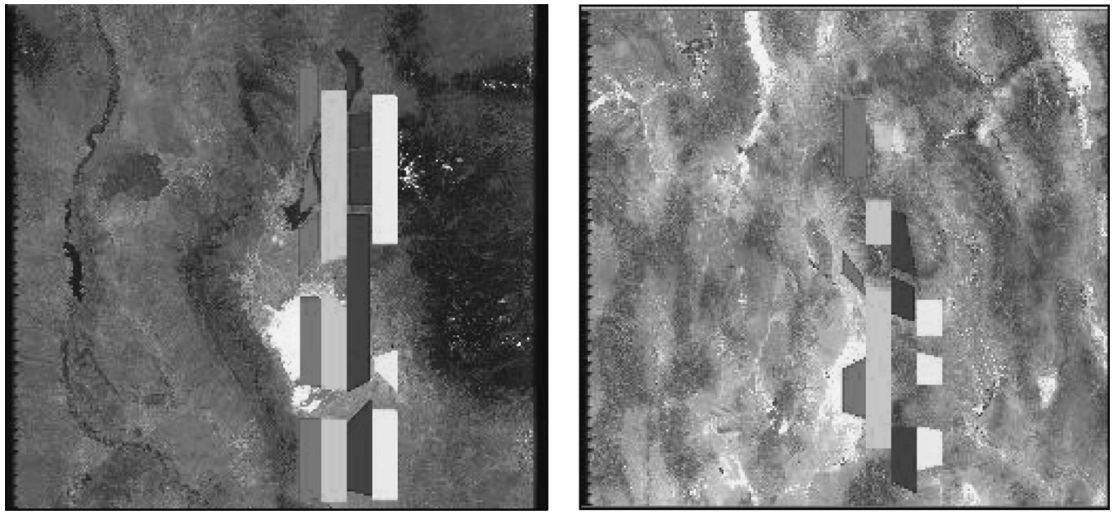

Fig. 3. Large areas common to ETM+ and ALI for the White Sands (DOY 084) and Railroad Valley scene (DOY 181).

the earth's surface radiance or the internal calibration lamps; the response is quantized into eight- (for ETM+) and 12-bit (for ALI) numbers that represent brightness values commonly called Digital Numbers. During L1 product generation, these numbers are converted to units of absolute radiance. This paper refers to measured radiance in this sense. To maintain consistency with ETM+, this paper uses spectral radiance units of watts per square meter per steradian per micron. Note that the conversion factor is 1 : 10 when going from milliwatts per square centimeter per steradian per micron units to watts per square meter per steradian per micron.

E. EO-1 ALI and L7 ETM+ Quantization

ALI L1R images were quantized to 12-bit radiometric resolution, providing greater dynamic range and improved sensitivity relative to the eight-bit resolution of ETM+. As a result, ALI can more accurately record radiances that might saturate ETM+. At least one of ETM+ images used in this analysis exhibited saturation effects in bands 5 and 7, whereas ALI exhibited no saturation in these bands over the same regions. Consequently, these regions were excluded from the analysis.

II. Calibration With Nearly Simultaneous Surface Observations

ALI was designed to serve as a candidate technology for Landsat data continuity. To evaluate ALI's capabilities in this role, a cross-calibration study was performed using image pairs coincidentally acquired with the ETM+ and ALI sensors; this study used two approaches. In the first approach, cross calibration was performed with image statistics based on large common areas observed nearly simultaneously by the two sensors. The scenes selected for this approach included the Railroad Valley Playa and White Sands. The Railroad Valley dry lake playa is very homogeneous and consists of compacted clay-rich latchstring deposits forming a relatively smooth bright surface compared to most land covers. Because the image acquisitions occurred within a 1-min window, it was assumed that the surface and atmospheric conditions did not change during that time.

A. Geometric Matching

Geometrically, the L7 and EO-1 sensors differ in their along-track and across-track pixel sampling. A feature simultaneously observed by both sensors will be represented by slightly different numbers of image pixels because of the differences in viewing geometry and sensor scanning times. This makes it very difficult to establish sufficient geometric control to facilitate radiometric comparisons on a point-by-point and/or detector-by-detector basis. Therefore, the analysis approach made use of image statistics based on large areas in common between the image pairs (a pair represents an acquisition of a nearly simultaneously observed area by each of the ALI and ETM+ sensors). These large areas were carefully selected using distinct features common to both of the images. Both bright and dark regions were selected to obtain maximum coverage over each sensor's dynamic range. ETM+ and ALI image pairs can be geometrically registered, but that involves resampling. For this particular study, any kind of resampling was avoided to obtain the highest radiometric accuracy without corrupting the pixels due to resampling. The use of large areas common to both the ETM+ and ALI image data successfully avoids radiometric effects due to residual image misregistration.

B. Regions of Interest

Regions of interest (ROIs) were selected within each respective SCA of the ALI and ETM+ scenes in order to understand the relative differences within SCAs. Areas common to the two images in a pair were selected to exclude clouds and cloud shadows. The regions were also selected to exclude ALI inoperable detectors determined by the Massachusetts Institute of Technology Lincoln Laboratory during prelaunch testing. To understand the relative differences between SCAs, the regions were selected to identify scene statistics specific to a given SCA. Fig. 3 shows the selected regions that were common to the ETM+ and the respective SCA of ALI for the White Sands and Railroad Valley test sites. The regions in left corner are the ground targets common to the ETM+ and SCA-4; then, ETM+

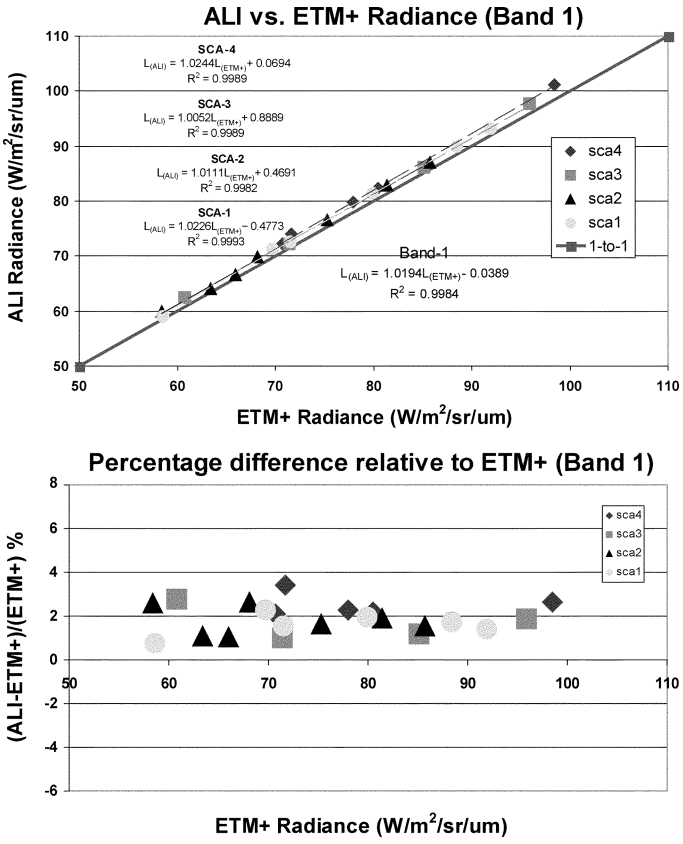

Fig. 4. Comparison of radiance obtained from large ground regions common to band 1 of both ALI and ETM+ sensors.

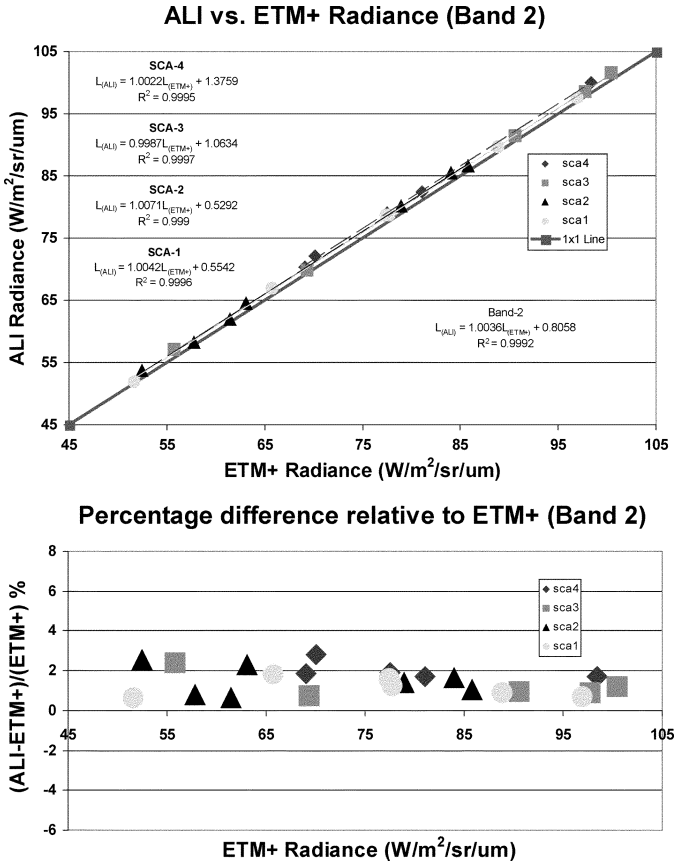

Fig. 5. Comparison of radiance obtained from large ground regions common to band 2 of both ALI and ETM+ sensors.

and SCA-3; then, ETM+ and SCA-2; and the right corner has the ground targets common to the ETM+ and SCA-1. Once all area ROIs were selected, image statistics were computed to obtain minimum, maximum, mean and standard deviation target values on a band-by-band basis. The mean target statistics from both sensors were then converted to absolute units of radiance, which is the first and fundamental step in putting image data from multiple sensors and platforms onto a common radiometric scale.

C. Hypothesis Test

The mean target statistics obtained from the ROI were converted to radiance. Cross-calibration results were tested for a slope value of 1.0 (corresponding to exact agreement in radiances between the two sensors) at a 0.001 significance level after fitting a regression line to data from the common ROIs. For ALI, the regression lines were determined for data within each SCA, as was an overall regression combing all data points from all SCAs.

D. Results and Discussions

The ALI bands that were designed to mimic the standard ETM+ spectral bands 1, 2, 3, 5, and 7 were used in this study. ETM+ band 4 was not taken into consideration because the respective spectral response in ALI was divided into two narrower bands, 4 and 4p. The radiance measurements obtained from the corresponding bands 1, 2, 3, 5, and 7 over the selected ROIs were compared; the results from these comparisons are summarized in Fig. 4–8. The upper plots in each of these figures relate radiances obtained from ETM+ data to corresponding radiance obtained from ALI data. Each data point on the plots represents an ensemble average of all pixels in a given ROI and color-coded by SCA. The ETM+ radiance is plotted on the x axis, and the ALI radiance is plotted on the y axis. The one-to-one line indicates perfect agreement between the radiance measurements obtained from both sensors for a particular band. The slope of the regression represents the gain ratio between the two sensors. The lower plots in Figs. 4–8 represent percentage differences in observation using ALI relative to ETM+ data. The ETM+ radiance is plotted on the x axis, and the percentage difference of the ALI radiance relative to ETM+ is plotted on the y axis. The radiance measurements obtained from ALI for the common spectral bands were found to closely match with the radiance measurements in the corresponding ETM+ bands.

Fig. 4 summarizes the radiance comparison results for band 1. The data points do not lie precisely on the one-to-one line. In the percentage difference plots, all data points lie above the one-to-one line, indicating that ALI is estimating a 1% to 3.5% higher radiance than ETM+. The overall slope of the regression line for band 1 is 1.019.

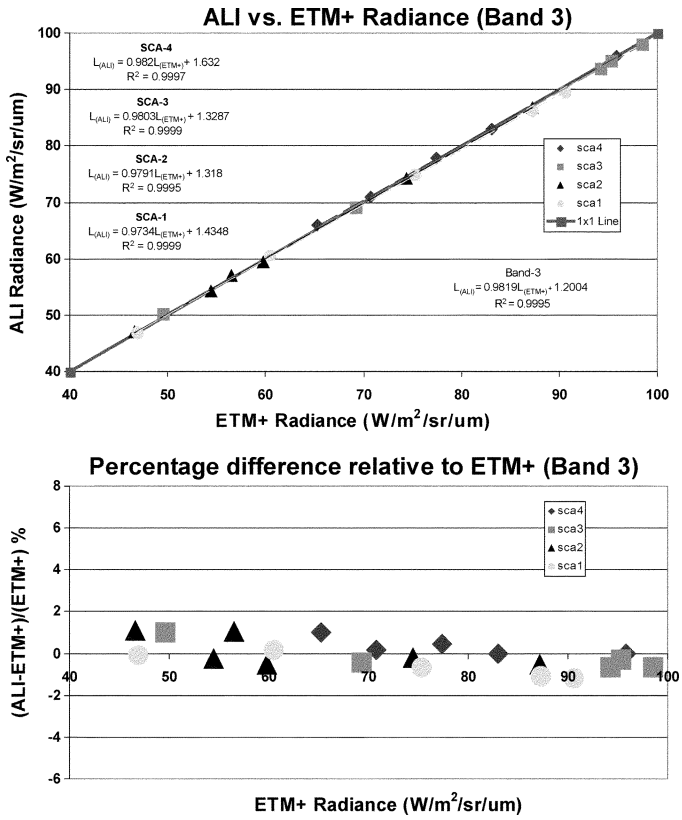

Fig. 6. Comparison of radiance obtained from large ground regions common to band 3 of both ALI and ETM+ sensors.

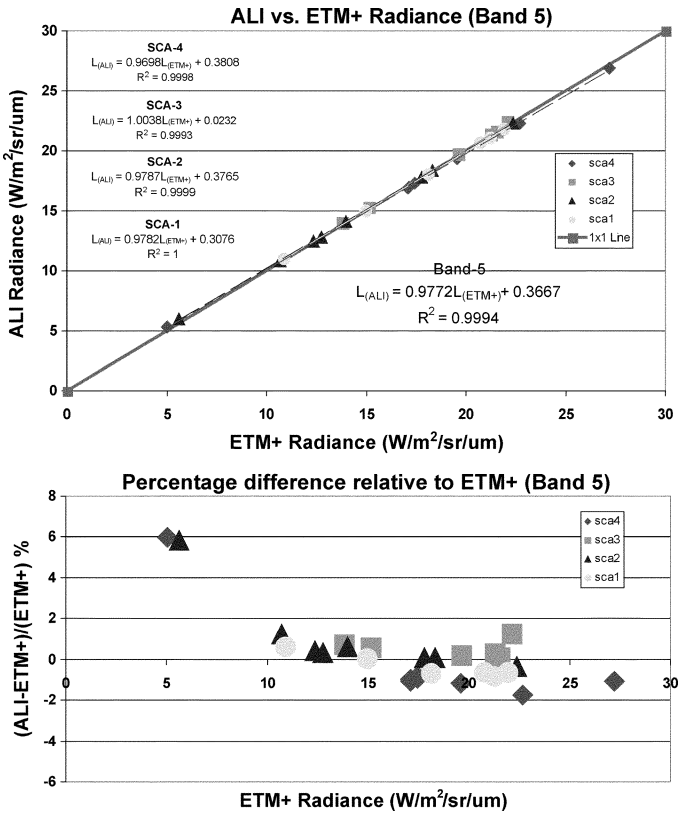

Fig. 7. Comparison of radiance obtained from large ground regions common to band 5 of both ALI and ETM+ sensors.

Fig. 5 summarizes the radiance comparison results for band 2. Again, ALI appears to be estimating a 1% to 2% higher radiance than the ETM+. The overall slope of the regression line for band 2 is 1.003.

Fig. 6 summarizes the radiance comparison results for band 3. All data points lie very near the one-to-one line, indicating excellent agreement in radiance estimates between the two sensors. The percentage difference plots suggest that ALI is estimating a 0.5% higher radiance than the ETM+ at lower signal levels, and approximately a 1.0% lower radiance at higher signal levels. However, it should be noted that there does not seem to be a large deviation in the radiance measurements. The overall slope of the regression line for band 3 is 0.981.

Fig. 7 summarizes the radiance comparison results for band 5. Two of the data points at lower signal level have a 6% difference relative to ETM+. These data points can be considered as outliers because at such low signal levels, there is not much absolute difference in the radiance measurements, and noise is more significant than the input signal. SCA-3 and SCA-2 appear to estimate a 0.7% higher radiance than the ETM+, while SCA-4 and SCA-1 appear to estimate a 1% lower radiance than the ETM+. The overall slope of the regression line for band 5 is 0.977.

Fig. 8 summarizes the radiance comparison results for band 7. The percentage difference plots show that all data points lie below the zero line, indicating that ALI is underestimating radiance in comparison to the ETM+. Each SCA behaves differently: SCA-4 appears to estimate up to a 1% lower radiance,

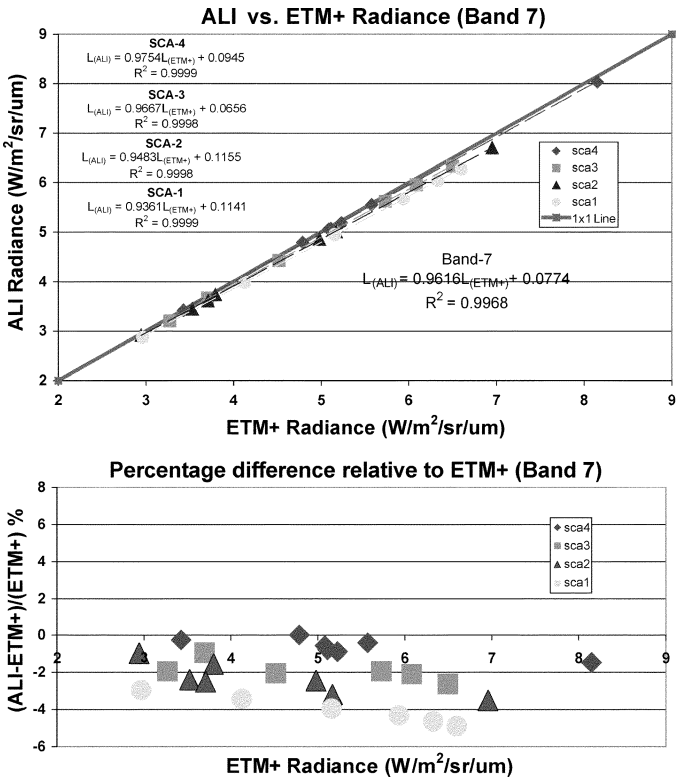

Fig. 8. Comparison of radiance obtained from large ground regions common to band 7 of both ALI and ETM+ sensors.

SCA-3 appears to estimate a 1% to 2% lower radiance, SCA-2 appears to estimate a 2% to 3% lower radiance, and SCA-1 appears to estimate a 3% to 4% lower radiance. The overall slope of the regression line for band 7 is 0.961.

TABLE IV
SLOPES FROM ALL THE REGRESSION LINES FOR DATA POINTS WITHIN EACH SCA AND THE COMBINED RESULTS FROM ALL DATA PLOTS BELOW FOR ALL OF THE BANDS

	Slope from the regression lines					% diff
Band	SCA4	SCA3	SCA2	SCA1	ALL	ALL
1	1.02	1.01	1.01	1.02	1.02	1.94
2	1.00	1.00	1.01	1.00	1.00	0.36
3	0.98	0.98	0.98	0.97	0.98	-1.81
5	0.97	1.00	0.98	0.98	0.98	-2.28
7	0.98	0.97	0.95	0.94	0.96	-3.84

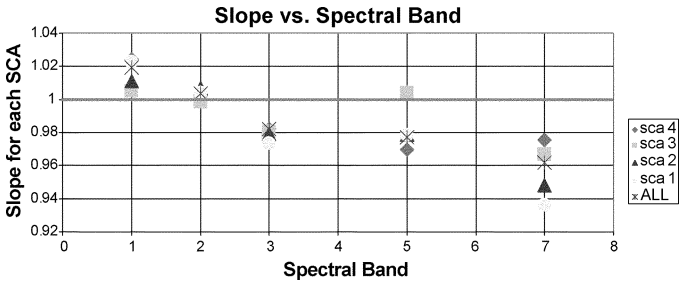

Fig. 9. Slope from the regression lines for data points within each SCA or each SCA with respect to ETM+ for the spectral band common to both ALI and ETM+ sensors.

The slopes from all the regression lines and the bands are summarized in Table IV. The null hypothesis for slope $= 1$ is tested at a significance level of $\alpha = 0.001$. The results indicated that the VNIR bands 1, 2, and 3 satisfy the null hypothesis, indicating good agreement between the relative SCA gains. The SWIR bands 5 and 7 reject the null hypothesis. One normally expects poorer performance at longer wavelengths where solar signal is low and detector materials are different. The slopes from all of the bands are plotted and summarized in Fig. 9. It can be observed from Table IV that the relative SCA gains agree with ETM+ VNIR bands within approximately 2% and the SWIR bands within approximately 4%. SCA gains in the VNIR bands are clustered together, showing that the relative SCA gains are well-matched and the SCA behaves similarly. The SCA gains in the SWIR bands behave differently, showing a more pronounced disagreement between the relative SCA gains.

III. VICARIOUS CALIBRATION

The second approach used for the cross-calibration study was vicarious calibration. Vicarious calibration techniques estimate the radiance seen at the sensor over a selected test site on the earth's surface. Assessment involved using a radiative transfer model to propagate surface measurements made at the time of the EO-1 and L7 overpass to predict the at-sensor radiance. The predicted radiance was then convolved with the respective sensors spectral response function to obtain the predicted radiance that was then compared with the measured radiance. In the summer of 2001, ground reference data were collected at the Brookings test site. A cloud-free scene acquired on September 5, 2001 (DOY 248) was used for this particular study. Again, the difference between acquisition times for both satellites was less than a minute, allowing for a direct comparison of imagery from both sensors.

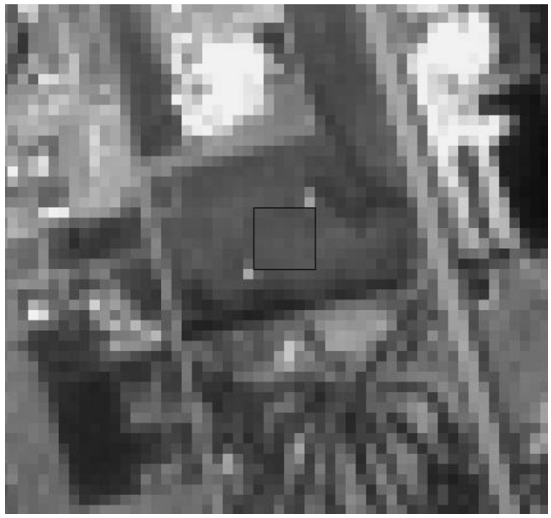

Fig. 10. Tarps serve as ground reference points for 180 × 180 m ground area. The area contains 6 × 6 multispectral band pixels.

The major advantage of the vicarious calibration approach is that surface measurements can be obtained at or near the overpass time. However, vicarious calibrations are labor-intensive, which limits the number of calibrations that can be performed. Another limiting factor is that calibrations can only be performed infrequently, when the sensor acquires data over the target test site. For ETM+/ALI, this means that the maximum number of calibrations possible during a given year, over a given test site, is 22. The actual number will almost certainly be smaller due to unfavorable sun angles and local weather conditions (such as cloud cover obscuring the test site).

A combination of both vicarious and onboard calibration methods is necessary for an accurate picture of the status of sensor response over time. The vicarious results give full-aperture, full-path calibrations with relatively high accuracy. The onboard system provides more frequent assessments of the sensor's behavior as a function of time over periods of hours to months. Beyond this period, it becomes necessary to verify the status of the onboard references (lamps, diffusers) through independent means. The vicarious methodology provides an independent check of onboard calibration over the life of the mission.

A. Target Area

Field data were collected in an open meadow at the Brookings test site. A target area of 180 × 180 m, as shown in Fig. 10, was centered in this meadow, which acted as a large, relatively flat, spatially homogeneous region. The ground sample distance for the ETM+ and ALI multispectral band is 30 m, so the target area shows up in the imagery in a 6 × 6 pixel window. On the morning of the overpass, the target area corners were flagged with two sets of three blue tarps (covering a 30 × 30 m rectangle) placed adjacent to pinpoint the exact location of the target in the satellite imagery.

TABLE V
PREDICTED TOA RADIANCE FOR THE ETM+ BANDS

Band-averaged Results		Sept. 05, 2001 (ETM+ Data)								
Filter	Wave Length	Optical Depths			Gaseous Trans	Omega	Surface Reflectance	Solar Irradiance	Relative Radiance	Absolute Radiance
		Aerosol	Molec.	Ozone						
L7-B1	0.479	0.173	0.166	0.006	0.998	0.906	0.048	1938.762	0.027	52.446
L7-B2	0.561	0.135	0.087	0.032	0.984	0.900	0.079	1813.168	0.025	43.831
L7-B3	0.661	0.104	0.044	0.018	0.962	0.893	0.091	1522.991	0.024	35.594
L7-B4	0.835	0.073	0.017	0.000	0.907	0.882	0.282	1027.550	0.066	61.205
L7-B5	1.650	0.025	0.001	0.000	0.907	0.843	0.320	222.164	0.075	15.187
L7-B7	2.208	0.016	0.000	0.000	0.826	0.822	0.181	80.760	0.043	2.888
L7-PAN	0.720	0.096	0.040	0.012	0.917	0.889	0.185	1347.740	0.045	50.283

TABLE VI
PREDICTED TOA RADIANCE FOR THE ALI BANDS

Band-averaged Results		Sept 05 2001 (ALI Data)								
Filter	Wave Length	Optical Depths			Gaseous Trans	Omega	Surface Reflectance	Solar Irradiance	Relative Radiance	Absolute Radiance
		Aerosol	Molec.	Ozone						
ALI-B1	0.485	0.170	0.157	0.008	0.998	0.906	0.050	1937.178	0.026	51.254
ALI-B1P	0.442	0.196	0.227	0.001	0.999	0.909	0.039	1821.637	0.031	56.528
ALI-B2	0.567	0.133	0.083	0.034	0.981	0.899	0.080	1808.470	0.024	43.324
ALI-B3	0.660	0.105	0.044	0.018	0.968	0.893	0.091	1527.465	0.024	35.747
ALI-B4	0.790	0.079	0.021	0.000	0.958	0.885	0.265	1146.674	0.062	68.451
ALI-B4P	0.866	0.069	0.015	0.000	0.988	0.880	0.293	940.666	0.069	63.796
ALI-B5	1.640	0.025	0.001	0.000	0.928	0.843	0.320	226.440	0.075	15.756
ALI-B5P	1.244	0.039	0.003	0.000	0.892	0.860	0.372	444.310	0.087	34.339
ALI-B7	2.226	0.016	0.000	0.000	0.823	0.821	0.180	78.383	0.042	2.822
ALI-PAN	0.592	0.126	0.075	0.027	0.984	0.898	0.080	1719.986	0.024	41.078

B. Field Instruments

The spectral measurements were obtained with Analytical Spectral Devices Full Range (ASD-FR) spectrometer that measures irradiance from 350–2500 nm. Upwelling radiance and reflectance were derived from these measurements. The ASD were used to take the spectra every 10 m along six north–south paths between 11:40 A.M. and 12:10 P.M. to coincide with the Landsat overpass at 12:02 P.M. and the EO-1 overpass 1 min later. One hundred and eight spectra were recorded that sampled the target area uniformly. These spectra were averaged to give the net reflectance spectrum of the entire target area. White panel spectra were recorded at the beginning, halfway through, and at the end of the 30-min data collection period. The spectralon reference panel (0.45×0.45 m) was calibrated for the bidirectional reflectance distribution function by the University of Arizona (UOA) Remote Sensing Group's Calibration Laboratory.

Down-welling spectral irradiance data were collected using two Multifilter Rotating "Shadow Band" Radiometers (produced by Yankee Environmental Systems). An important observational data parameter obtained from these shadow band measurements is the diffuse-to-global ratio, which is very sensitive to solar geometry, average surface reflectance, aerosol extinction, and scattering phase function. The diffuse-to-global ratios were measured at five wavelengths by two automated shadow band radiometers recording measurements at the time of the overpass. One radiometer was operated from the roof of Crothers Engineering Hall on the South Dakota State University (SDSU) campus, approximately 3 km from the target site. The other unit was operated at the target site.

Atmospheric transmittance was monitored and evaluated using an automated Reagan ten-channel sun photometer. The sun photometer recorded observations of direct solar irradiance in 1-min intervals from sunrise to sunset, providing morning and afternoon Langley plots at ten wavelengths (10-nm bandwidths). For the day of interest, the Langley plots also indicated that the sky conditions remained stable throughout the day.

C. Atmospheric Characterization

The method used to perform the vicarious calibrations was a reflectance-based approach, in which results of ground field measurements made with the instruments were used as constraints in creating a subsequent radiative transfer code. The modeling effort used the optical depth data obtained from the sun photometer and iterative simulations to replicate the observations as recorded by the ground-level instruments. Then, having satisfactorily reproduced those conditions, the model was used to predict radiances at the satellite sensor altitude. The background information and processing methodology have been generated and reported elsewhere. References at the end of this paper should be used for additional information [3]–[6].

Tables V and VI presents the extinction coefficients (vertical optical depths at one air mass) estimated from the morning and evening Langley plot data and the instantaneous measurements at the time of the overpass; postprocessing of the data resulted in optical depth estimates separated into the following components: molecular optical depth, aerosol optical depth, and ozone optical depth. The instantaneous values were derived from a 5-min average of the observed solar irradiance at the time of the overpass. The at-sensor predicted radiance for all of the ETM+ and ALI bands is also summarized in the table.

TABLE VII
STATISTICS OBTAINED FROM 180 × 180 m AREA. (a) L7 ETM+ BANDS. (b) EO-1 ALI BANDS

(a)

Units: DN				
Band	**Min**	**Max**	**Mean**	**Stdev**
1	4930	5588	5224.58	140.14
2	4289	4759	4474.42	104.08
3	3274	3944	3640.56	166.38
4	5901	6786	6272.81	206.93
5	1399	1537	1460.89	33.49
7	252	299	274.03	11.31

(b)

Units: DN				
Band	**Min**	**Max**	**Mean**	**Stdev**
1	1725	1777	1750.47	13.35
2	1566	1622	1594.61	15.29
3	1298	1390	1342.03	23.99
4	1009	1137	1081.83	36.98
5	1972	2252	2081.81	72.39
6	1817	2072	1917.17	63.74
7	961	1056	1001.08	21.28
8	424	456	439.58	8.09
9	77	87	81.89	2.64

TABLE VIII
PREDICTED AND MEASURED RADIANCE IN WATTS PER SQUARE METER PER STERADIAN PER MICRON. (a) L7 ETM+ BANDS. (b) EO-1 ALI BANDS

(a)

Band	**Predicted (TOA) Radiance**	**Measured Radiance**	**% Difference**
1	52.45	52.25	0.38
2	43.83	44.74	-2.04
3	35.59	36.41	-2.23
4	61.21	62.73	-2.43
5	15.19	14.61	3.96
7	2.89	2.74	5.38

(b)

Band	**Band**	**Predicted (TOA) Radiance**	**Measured Radiance**	**% Difference**
1p	1	56.53	58.35	-3.12
1	2	51.25	53.15	-3.57
2	3	43.32	44.73	-3.15
3	4	35.75	36.06	-0.87
4	5	68.45	69.39	-1.36
4p	6	63.80	63.91	-0.17
5p	7	34.34	33.37	2.91
5	8	15.76	14.65	7.53
7	9	2.82	2.73	3.38

D. Results and Discussions

The target areas were easily located by visually observing the pixels brightened by the blue tarps, as shown in Fig. 10. Checks of adjacency effects were completed to determine if the starps affected the nearest nontarp pixels, and if the test site pixels were significantly different from adjacent nonsite pixels. It was found that the target area was relatively homogeneous and that the test site pixels were not significantly different from the adjacent pixels. For each band, the image statistics were computed for the counts within a 6 × 6 pixel window to get minimum, maximum, mean and standard deviation target values. The resulting statistics for ETM+ and ALI are summarized for each band in Table VII.

The measured radiance for ETM+ were computed from the mean target value obtained from the 6 × 6 pixel window in Table VII(a). Table VIII(a) summarizes the at-sensor predicted and measured radiance estimated for ETM+. Fig. 11(a) shows that there is a strong agreement between the predicted and measured ETM+ at-sensor radiances, indicating good characterization by the vicarious techniques. All of the points lie very near the one-to-one line. The best results were obtained for band 1, with a 0.38% difference, and the worst results were observed for band 7, with a 5.38% difference.

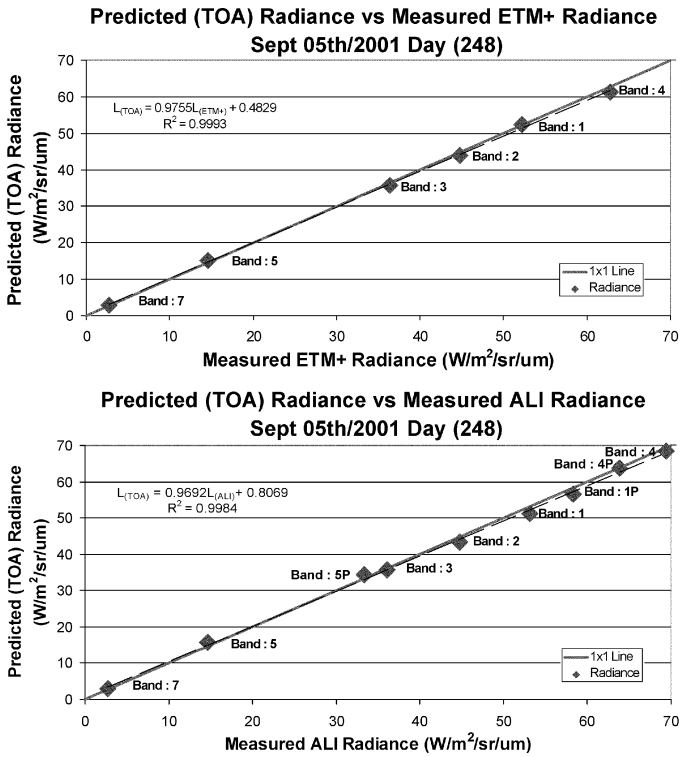

Fig. 11. Comparison of predicted radiance from ground truth measurements to the measured radiance obtained from both ALI and ETM+ sensors.

TABLE IX
MEASURED RADIANCE IN WATTS PER SQUARE METER PER STERADIAN PER MICRON. L7 ETM+ AND EO-1 ALI BANDS

ETM+ and ALI Bands	**Measured Radiance (L7 ETM+)**	**Measured Radiance (EO-1 ALI)**	**Percentage Difference**
1	52.25	53.15	1.74
2	44.74	44.73	-0.02
3	36.41	36.06	-0.95
5	14.61	14.65	0.30
7	2.74	2.73	-0.39

The measured radiance for ALI was computed from the mean obtained from the 6 × 6 pixel window in Table VII(b). Table VIII(b) summarizes the at-sensor predicted and measured radiance estimated for the ALI bands, as shown in Fig. 11(b). As with the ETM+ results, there is good agreement between the at-sensor predicted and measured ALI radiances. The best results were obtained for band 4p, with a −0.17% difference, and the worst results were observed for band 5, with a 7.53% difference. Table IX summarizes the measured radiance for a direct comparison between the ETM+ and ALI sensors estimated for each target area. Fig. 12 indicates good agreement between the two measurements; the data essentially lies on the one-to-one line.

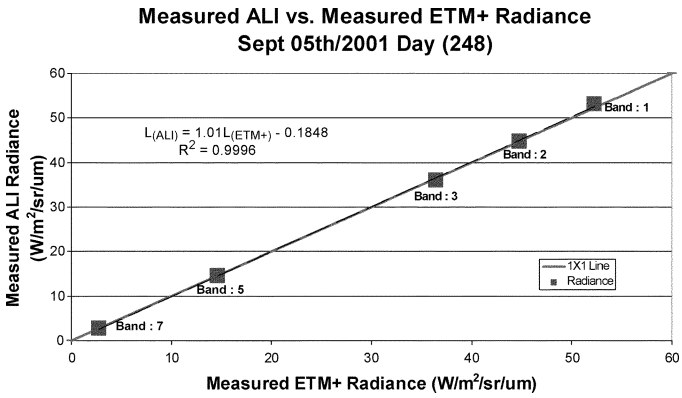

Fig. 12. Comparison of measured radiance obtained from the tarp region common to both ALI and ETM+ sensors.

Fig. 12 shows the percentage difference between the predicted and measured radiances obtained from the ETM+ and ALI spectral bands. Fig. 13(a) shows that the vicarious calibration results indicate differences of less than 4% for all ETM+ bands except band 7, which indicates a difference of 5.38 %. Fig. 13(b) shows that the vicarious calibration results indicate differences of less than 4%for all ALI bands except band 5, which shows a difference of 7.53 %. Fig. 13(c) shows the percentage difference between the measured radiances obtained from the spectral bands common to both ALI and ETM+ instruments. For this particular acquisition and the target area, the variation in the measured radiance was less than 2%.

It can be observed from Fig. 13(a) and (b) that both the ETM+ and ALI VNIR bands exhibit measured radiance higher than the predicted radiance, resulting in a downward trend of 0% to 3% for the ETM+ bands and 0% to 4% for the ALI bands. However, both the ETM+ and ALI SWIR bands exhibit measured radiance lower than the predicted radiance, resulting in an upward trend of 4% to 5% for the ETM+ bands and 3% to 7.5% for the ALI bands. Overall, the VNIR band results were within 4%, and the SWIR band differences were within 7.5 %. The comparison between the ALI and ETM+ atmospherically corrected satellite-based radiance estimates suggests that data continuity in the VNIR bands between the two sensors is excellent. Results from this campaign are generally consistent with results obtained from other field campaigns—both sensors could benefit from regular vicarious calibration campaigns. Clearly, further campaigns are necessary to establish a consistent calibration between ETM+ and ALI.

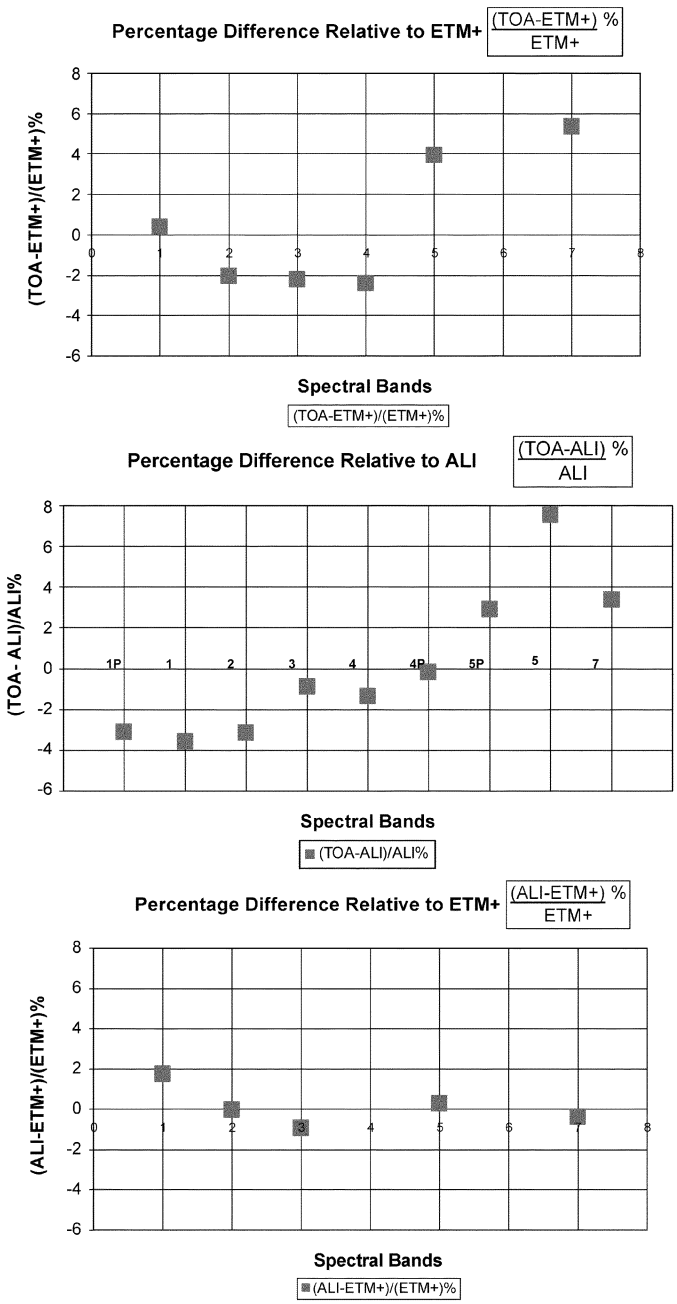

Fig. 13. Percentage difference between the predicted and measured radiance obtained from the spectral bands common to both ALI and ETM+ sensors.

IV. Summary

Cross calibration was performed between ETM+ and ALI image pairs using two approaches. One approach was based on image statistics of large common areas between the image pairs. The other approach was based on vicarious calibration that compares the measured radiance obtained from the sensor to the predicted at-sensor radiance using the surface measurements propagated to the sensor via radiative transfer code. The results from the radiometric comparison indicate that the SCA gains agree with the ETM+ VNIR band gains to within 2% and with the SWIR bands to within 4%. The agreement between SCA gains is better among the VNIR bands than among the SWIR bands. The vicarious calibration results indicate differences of 5.3% for all ETM+ bands and 7.5% for ALI bands for the September 5, 2001 (DOY 248) data.

Acknowledgment

Special thanks are extended to D. Aaron (SDSU) for his help at the Brookings test site. Surface reflectance spectra, optical parameters, and at-sensor predicted radiance measurements were kindly provided by K. Thome (UOA). Special appreciation is

given to M. Choate (EDC), and J. Barker (Goddard Space Flight Center) for information and feedback.

REFERENCES

[1] W. E. Bicknell, C. J. Digenis, S. E. Forman, and D. E. Lencioni, "EO-1 Advanced Land Imager," *Proc. SPIE*, vol. 3750, pp. 80–88, July 1999.

[2] P. M. Teillet, J. L. Barker, B. L. Markham, R. R. Irish, G. Fedosejevs, and J. C. Storey, "Radiometric cross-calibration of the Landsat 7 ETM+ and Landsat-5 TM sensors based on tandem data sets," *Remote Sens. Environ.*, vol. 78, no. 1–2, pp. 39–54, 2001.

[3] S. E. Black, D. L. Helder, and S. J. Schiller, "Irradiance-based cross calibration of Landsat-5 and Landsat 7 Thematic Mapper sensors," *Int. J. Remote Sens.*, vol. 24, no. 2, pp. 287–304, 2003.

[4] K. J. Thome, "Absolute radiometric calibration of Landsat 7 ETM+ using the reflectance based method," *Remote Sens. Environ.*, vol. 78, pp. 27–38, Oct. 2001.

[5] K. J. Thome, B. G. Crowther, and S. F. Biggar, "Reflectance and irradiance based calibration of Landsat-5 Thematic Mapper," *Can. J. Remote Sens.*, vol. 23, pp. 309–317, 1997.

[6] M. S. Moran, R. Bryant, K. Thome, W. Ni, Y. Nouvellon, M. P. Gonzalez-Dugo, J. Qi, and T. R. Clarke, "A refined empirical line approach for reflectance factor retrieval from Landsat-5 TM and Landsat 7 ETM+," *Remote Sens. Environ.*, vol. 78, pp. 71–82, 2001.

Gyanesh Chander received the M.S. degree in electrical engineering from South Dakota State University, Brookings, in 2001.

He is currently a Scientist with Science Applications International Corporation (SAIC) at the Earth Resources Observation System Data Center, U.S. Geological Survey, Sioux Falls, SD. He works on radiometric characterization and calibration of satellites and airborne instruments.

David J. Meyer received the B.S. and M.S. degrees in physics from Indiana State University, Terre Haute, in 1979 and 1984, respectively, and the Ph.D. degree in atmospheric science from the University of Michigan, Ann Arbor, in 1994.

He is currently a Principal Scientist with Science Applications International, Corporation, working at the Earth Resources Observation System Data Center, U.S. Geological Survey, Sioux Falls, SD, where he specializes in the characterization and application of airborne and spaceborne electro-optical imaging systems. His current research interests are vicarious calibration, radiation transport modeling, and atmospheric correction of remotely sensed data.

Dennis L. Helder (S'88–M'90) received the B.S. degrees in animal science and electrical engineering, the M.S. degree in electrical engineering from South Dakota State University, Brookings, and the Ph.D. degree in electrical engineering from North Dakota State University, Fargo, in 1979, 1980, 1985, and 1991, respectively.

For the past ten years, he has worked extensively with the Earth Resources Observation System Data Center, the National Aeronautics and Space Administration's Goddard Space Flight Center (GSFC), and Stennis Space Center in the area of radiometric, geometric, and spatial calibration of satellite imagery. Other activities include consulting, membership on the international Committee of Earth Observation Satellites Infrared, Visible, and Optical Sensor's subcommittee, a Visiting Scientist appointment at GSFC, development of the Landsat-7 image assessment system with GSFC, and design of aircraft imaging systems.